

pubs.acs.org/bc Article

Development of Red-Emissive Carbon Dots for Bioimaging through a Building Block Approach: Fundamental and Applied Studies

Keenan J. Mintz,[#] Emel Kirbas Cilingir,[#] Giacomo Nagaro, Suraj Paudyal, Yiqun Zhou, Durga Khadka, Sunxiang Huang, Regina M. Graham, and Roger M. Leblanc*



Cite This: Bioconjugate Chem. 2022, 33, 226–237



ACCESS I

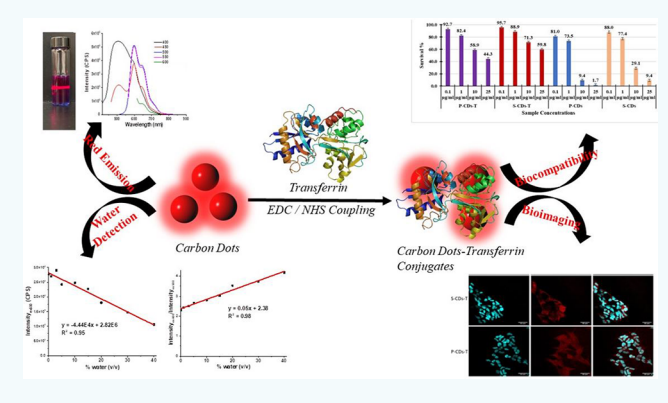
III Metrics & More

Artic

Article Recommendations

Supporting Information

ABSTRACT: In recent years, many researchers have struggled to obtain carbon dots (CDs) that possess strong photoluminescence in the red region of light. Success in this area has been limited, although the past few years have brought several promising reports on this topic. The most successful efforts in this area still seem to struggle from a lack of dispersibility/reduced emission in water. This work endeavors to understand the formation process of CDs that do not possess strong performance in an aqueous environment and to improve their capabilities in bioimaging. *ο*-Phenylenediamine (*ο*-PDA) is used along with various precursors in several different solvents (varying acidic and oxidative strengths) to understand the formation process behind the structure leading to red emission that is sensitive to water. These results showed that the combination of acid properties and oxidation is essential for this



process, and the important reactions are oligomerization of *o*-PDA and the crosslinking of these oligomers to form aromatic structural segments of CDs. These CDs are shown to be capable of quantitatively detecting water in organic solvents. Additionally, we have shown that conjugation with transferrin remarkably enhances the biocompatibility of these CDs. Transferrin-conjugated CDs with better biocompatibility were applied to bioimaging studies of neuroblastoma cell lines with N-*myc* and non-N-*myc* gene amplification, for the first time. Furthermore, CDs showed versatile bioimaging capability toward a highly aggressive neuroblastoma subgroup of tumors. The importance of creating red-emissive CDs has been well established, and this work is an important step toward understanding their formation and realizing their use in biological systems.

■ INTRODUCTION

In the last 20 years, carbon dots (CDs) have become a widely researched material in the areas of nanomedicine and bioimaging. 1,2 They can be defined as spherical, carbonbased nanoparticles with sizes between 1 and 10 nm, which have very promising optical properties and an easily modified surface.^{3,4} These properties have naturally suggested the application of CDs in biological areas and created the attention from scientists around the world. The optical properties of CDs are particularly promising as they commonly display an unusual property of excitation-dependent photoluminescence (PL), which creates versatility in choosing an optical window for any particular application.⁵ A common deficiency of CDs is their lack of emission/low quantum yield (QY) in the red region of light (above 650 nm), and this creates a challenge for imaging in biological systems as there is a great deal of autofluorescence and absorbing biological molecules in the blue region of light in which CDs typically emit the brightest PL.³

The production of CDs with red or near-infrared emission has been a longstanding goal, and recent years have produced some positive reports.^{5–8} These can be largely divided into two categories: strategies which use dyes possessing red emission and strategies which utilize small, aromatic molecules as "building blocks" for creating more conjugated products. Strategies involving dyes need to address the challenge of using enough energy to induce a reaction among the precursors and form CDs without making conditions harsh enough to completely destroy the structure of the precursor. Success in these efforts has been limited but has produced some CDs with long-wavelength PL.^{9–11} Accounts of these results may offer differing explanations, but the long-wavelength emission most likely results from incorporation of the dye (or a moiety of the dye) structure onto the surface of the CDs. Additionally, these products do not show the maximum emission from the red

Received: November 18, 2021 Revised: December 2, 2021 Published: December 16, 2021





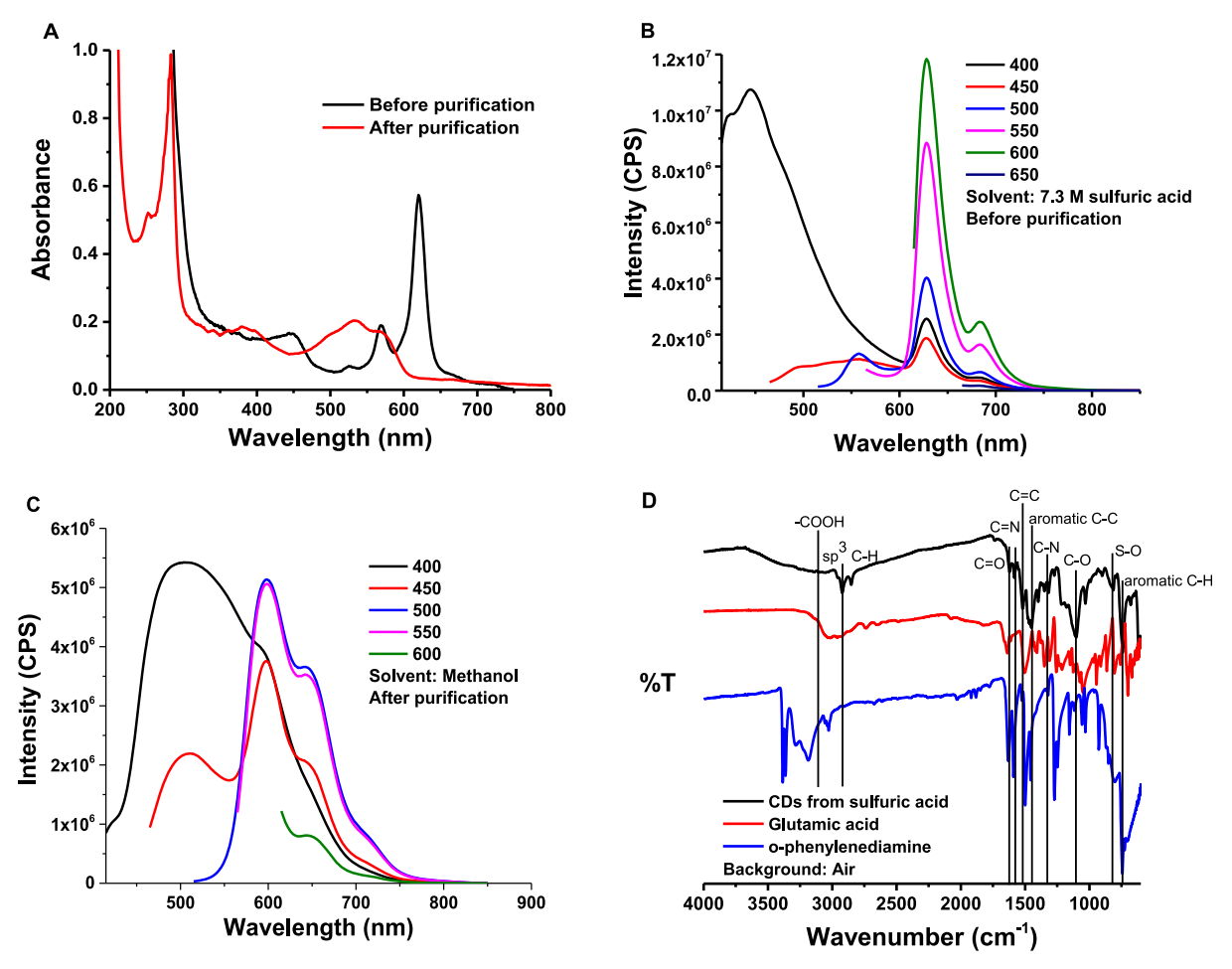


Figure 1. (A) Absorption spectra of S-CDs before (solvent 7.3 M sulfuric acid) and after purification (solvent: methanol). (B) PL spectra for S-CDs before purification. (C) PL spectra for S-CDs after purification. (D) Fourier-transform infrared (FTIR) spectra for S-CDs and their precursors.

region, as the traditional emission for CDs from the blue region of light dominates the spectra (when these data are presented). In terms of bioimaging, this is only an incremental improvement over many CDs.

The second area involving small, aromatic molecules has shown more success in this regard, but different challenges have emerged concerning water dispersibility. Several studies have claimed a high performance in water for their respective systems, but questions have been raised concerning reproducibility through published studies and work in our own lab.^{7,12–14} Many of these reactions take place in nonaqueous environments conducive to the building of larger organic systems, so it is unsurprising that these CDs would struggle with a lack of dispersibility/emission in water. This strategy produces brighter emission than strategies involving dyes, but if this is to be a viable approach for biological applications, the performance in water must be improved.

The CDs produced in this study are evaluated for their bioimaging capabilities in neuroblastoma subgroup tumor in vitro models. Neuroblastoma is defined as a cancer of the peripheral nervous system that almost exclusively occurs during early childhood. Neuroblastoma is responsible for 6–10% of all childhood tumors along with 12–15% of all cancer-related deaths in children. It is an extracranial solid tumor, and its mean age of diagnosis is 17–18 months. Forty percent of the patients diagnosed with neuroblastoma are

younger than 1 year, and less than 5% of the patients are older than 10 years verifying neuroblastoma as the most common and deadly tumor for infants.¹⁷ Compared to adult tumors, pediatric cancers usually advance during a much shorter timeperiod along with less genetic abnormalities. Several of these childhood tumors possess embryonal characteristics that are most probably triggered by abnormalities in genes and/or deregulated expression of genes. 18 The prognosis rate for neuroblastoma is extremely poor for patients over 18 months of age with metastatic disease despite intensive treatment with chemotherapy, surgery, and radiotherapy. 19,20 One of the most common chromosomal abnormalities related to this poor prognosis in neuroblastoma is N-myc gene amplification. 15 It has been shown that high-risk neuroblastoma subgroups of tumors with survival rates less than 50% have a higher chance to be developed with the presence of N-myc gene amplification. 15 Even though there are studies to understand the biological features of neuroblastoma cell lines with N-myc gene amplification and non-N-myc gene amplification, there is a vast need of improvement for the materials which are applied to diagnostic and treatment trials of these neuroblastoma subgroups of tumors regarding their water solubility, PL property, and biocompatibility. Thanks to their intrinsic properties such as high biocompatibility, good water solubility, and excellent PL, CDs can be designed to provide desired improvements for these materials. To the best of our

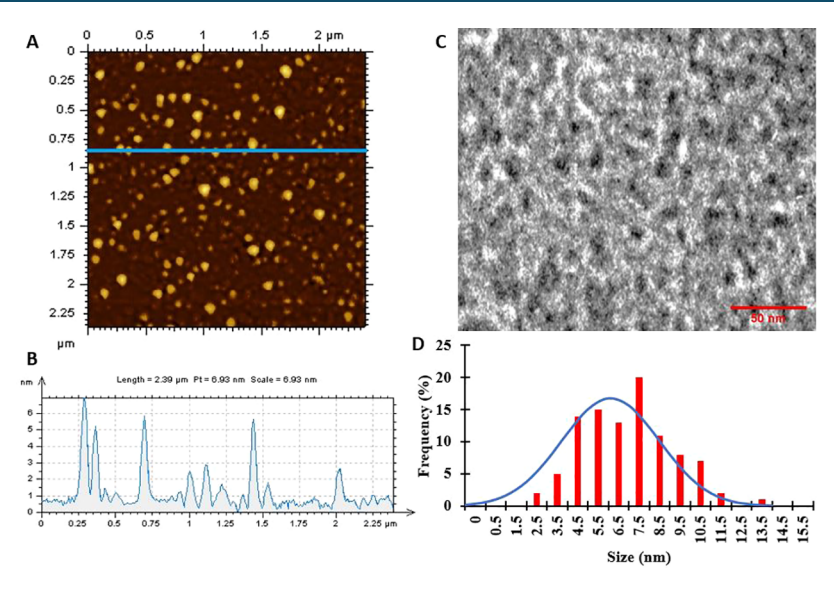


Figure 2. (A) AFM image for S-CDs and (B) extracted height profile. (C) TEM image for S-CDs. The scale bar is 50 nm. (D) TEM histogram of S-CDs fitted with gaussian size distribution.

knowledge, bioimaging of CDs for different neuroblastoma cell lines with or without N-myc gene amplification has not been studied before. Elaborate investigation of neuroblastoma cell lines with and without N-myc gene amplification has upmost significance to have better understanding about the nature of neuroblastoma and eventually design improved strategies for the diagnostic and treatment trials. In this study, we compared bioimaging capabilities of our prepared CDs with one N-myc gene-amplified neuroblastoma cell line SMS-KCNR and one non-N-myc gene-amplified neuroblastoma cell line SK-N-AS.

This study builds upon a previous strategy to better understand the formation of red emission from organic building blocks and improve the properties of these CDs in water. Several different acids are used as solvents, and various precursors are used to reveal a potential mechanism for the prepared CDs. o-Phenylenediamine (o-PDA) and glutamic acid are used as precursors with sulfuric acid and phosphoric acid to produce S-CDs and P-CDs, respectively. These two CDs are tested in various cell lines and also conjugated with transferrin, which is shown to significantly increase the biocompatibility of the CDs. Finally, the promising bioimaging ability of S-CDs and P-CDs in one N-myc gene-amplified neuroblastoma cell line SMS-KCNR and one non-N-myc geneamplified neuroblastoma cell line SK-N-AS is displayed.

■ RESULTS AND DISCUSSION

After the reaction with 7.3 M sulfuric acid, the solution was a dark green/blue color and upon neutralization developed a red/brown color with a precipitate. When a green laser was held up to the reaction before purification, red PL could be seen on the surface of the solution, but this disappeared upon neutralization. For this reason, optical characterization was performed on the sample before purification (solvent: 7.3 M $\rm H_2SO_4$), the supernatant after centrifugation (solvent: water), and the precipitate after purification (solvent: methanol).

Optical Properties. The absorbance properties of S-CDs were examined before and after purification (Figure 1A). The sample before purification shows excessive UV absorption, which is unsurprising given that the precursors and water-dispersible byproducts absorb in this range. After purification, the sample shows a very sharp peak just below 300 nm

indicating the transition between the π states of C=C bonds. More significantly for this work, both samples show absorption at wavelengths longer than what is typically seen for CDs, although the peaks are quite different before and after purification. The differences at long wavelengths can be attributed to a solvent effect, as the purified product was redissolved in acid and showed a similarly sharp peak at 620 nm, while those at shorter wavelengths are related to the removal of the unreacted precursor and water-dispersible CDs.

Similar differences occur in the PL spectra before and after purification which can again be attributed mostly to the solvent effect (Figure 1B and C). A blue shift is seen after purification as the long-wavelength emission maximum shifts from 630 to 600 nm. Additionally, a new shoulder arises above 700 nm after purification. The change in the sharpness of the absorption peaks and the new absorption shoulder can be attributed to the change in protonation after removal of the strong acid. Similar to the absorption spectra, an increase in breadth can be seen for the purified samples as the full width at half maximum (FWHM) is much larger than that for the unpurified sample (Figure 1B,C). The lack of protonation expected from methanol could lead to a more varied electronic structure thus increasing the width of the purified S-CDs' peaks, while the less polar environment leads to the blue shift as has been observed for CDs previously. ^{23,24} To examine this hypothesis, the optical properties of S-CDs were recorded in different solvents (Figure S1). The difference between methanol and sulfuric acid is clear, as previously discussed, but in lower polarity solvents (acetone and THF), the absorbance and PL are blue-shifted about 40 nm. Similar spectra observed for acetone and THF suggest that hydrogen bond donation is the greater determination of S-CDs' optical properties than polarity. For both the unpurified and purified samples, emission in the blue region is strong and on the same scale as the emission from the red region. The fact that this peak remains, even after removing water-soluble impurities, suggests that there are two mechanisms within the S-CD samples. The emission from the blue region most likely comes from the localized states which are well defined for carbon materials and arise from defects and distortions in the carbon structure. 14,25 The mirroring of the absorbance and PL spectra

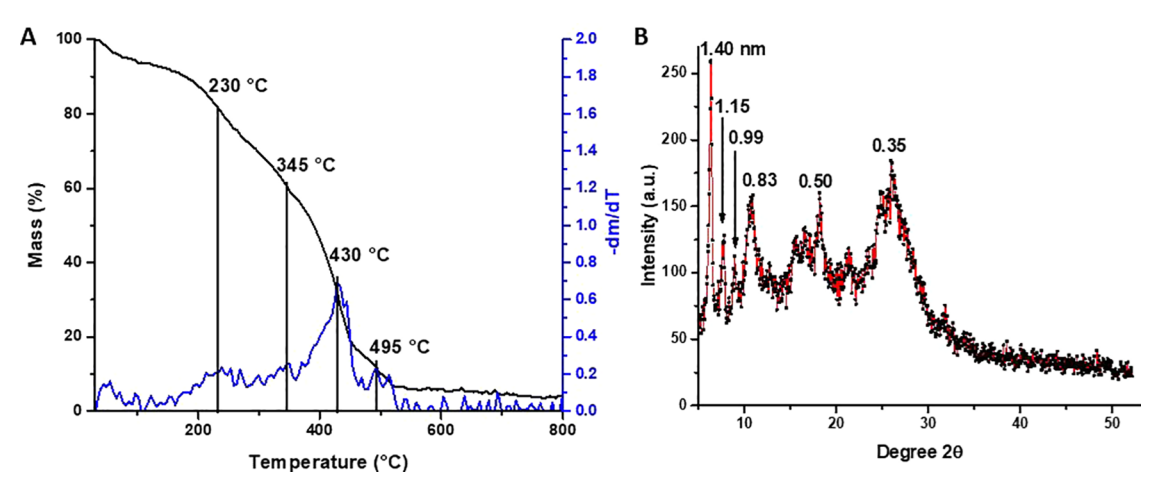


Figure 3. (A) Thermogram for S-CDs. (B) XRD pattern for S-CDs and the corresponding d-spacing for each peak is labeled in nanometer.

before purification suggests a molecular type of mechanism although this is less clear after purification but appears to still be present. Additionally, QY measurements were performed, and the calculated value for S-CDs was around 9.8%. In the literature, existing red-emissive CDs show QY percentages from 1 to 53%, but the majority of existing red-emissive CDs possess QY values which fall from 2 to 8%. 26 From this point, S-CDs exhibited a QY value that is above the majority of the existing examples. Therefore, S-CDs can be considered as promising candidates for biological applications such as cellular bioimaging studies. The emission region of S-CDs is desirable for biological applications, but their solubility properties are not ideal as they display little dispersibility/emission in pH neutral aqueous media. Further work was performed, however, to first examine the effect which allows the reaction in acid to produce red emission, and second to exploit the enhancement of the emission properties in organic and acidic solvents.

Structure and Morphology of S-CDs. The FTIR spectra of S-CDs and their precursors show appropriate changes one would expect after treatment with acid under harsh conditions (Figure 1D). S-CDs show typical functionalization including -COOH and -C=O groups, but more importantly, peaks related to aromatic carbon at 1450 and 750 cm⁻¹ (C-C and C-H, respectively) as well as C-N and C-O bonding. The groups indicated here support the construction of sp² networks as being a possible factor for the development of this orange/ red emission although more work should be performed to demonstrate this. Additionally, the peak indicating -COOH groups is muted compared to other CDs and may explain the lack of water dispersibility for S-CDs. 27 Surface potential of S-CDs was also calculated as -3.7 mV in methanol which further confirms the lack of -COOH groups as the reason for the low dispersibility in water. To evaluate the height of the particle, atomic force microscopy (AFM) was performed to show S-CDs that were between 3 and 6 nm and in the range typically seen for CDs (Figure 2A,B). On the other hand, we observed a relatively wider and asymmetric gaussian size distribution between 2 and 12 nm for the transmission electron microscopy (TEM) images (Figure 2C,D). As a result of two microscopic techniques, we concluded that S-CDs have a roughly spherical shape and a mean particle size around 6-8 nm. Thermogravimetric analysis (TGA) was performed to provide some structural information (Figure 3A). The very small drop in mass from evaporation of water at the beginning of the thermogram correlates with the lack of affinity of S-CDs for

water. The change in masses observed between 200 and 350 °C most likely results from surface functional groups, including –COOH groups. ^{28,29} The mass loss above 400 °C is likely due to the decomposition of the core. The lower thermostability observed here than for other previously reported CDs may arise from a segmentation of sp² sections by glutamic acid, resulting in a hybrid sp²/sp³ structure with lower thermostability as observed. ³⁰ The arrangement of these structures into spherical particles may preserve the emission of the aromatic regions by providing spacing between the emissive regions and avoiding quenching through energy transfer.

The X-ray diffraction (XRD) pattern of S-CDs (Figure 3B) reveals similar traits to what is commonly seen for CDs, as well as some variation. The peak at 26° (corresponding to a dspacing of 0.35 nm) is what is commonly seen for CDs and roughly correlates to graphitic spacing seen for graphite and carbon nitride sheets. 31,32 The slightly larger spacing (0.35 nm compared to 0.335 nm) is related to the confinement of the lattices in a small particle and the presence of heteroatoms. Most of this XRD pattern shows broad peaks typical of amorphous materials, but interestingly, the peaks at smaller angles are much sharper indicating a higher degree of order or crystallinity. In our previous work, different CDs were observed with varying degrees of order, but one system showed a high degree of order (yellow CDs, Y-CDs).27 This system was also based on o-PDA but used a much more gentle technique (ultrasonication) than is used in this study, so the crystallinity is reduced for S-CDs because of graphitization but still retains some of the ordering from the use of this molecule. Spacings related to 0.5 and 1 nm were important for Y-CDs, as they corresponded to the length of o-PDA oligomers of varying lengths. For S-CDs, the broader peaks are related to lattices which have been graphitized and are only connected through π stacking and other noncovalent forces, while the sharper peaks most likely come from spacings between lattices which have o-PDA oligomers of 1-3 units connecting them and precisely determining the spacing.

When XRD patterns display sharp, narrow peaks, it is an indication that the powder possesses submicrometer crystals and the size of these crystals can be calculated from the FWHM according to the Scherrer equation.³³ This equation is commonly shown as: $\tau = \frac{K\lambda}{\beta\cos\theta}$; where K is a unitless factor which can be approximated as 0.9, λ is the X-ray wavelength, β is the FWHM in radians, and θ is the angle of the XRD peak

(Bragg angle). This calculation was performed for the two peaks at 6.3 and 7.6° , as their FWHM was most clear, and they were not unduly broad. These two calculations gave values of 19.5 and 20.6 nm indicating that S-CDs form crystals of approximately 20 nm in the powder form. This is an important detail, considering the low dispersibility of these particles in water, and they may play a role in in vitro testing. Based on the size determined from AFM and TEM ($\sim 3-8$ nm), this crystal size indicates that the CDs self-assemble into larger structures upon removal of solvent into the dried powder.

Change of Precursors and Solvents. This technique to prepare CDs raised many questions regarding the importance of precursors and/or solvent that we sought to answer. First, various precursors were used in place of glutamic acid to discern the role of the precursor. As can be seen in Table 1,

Table 1. Table Summarizing the Optical Properties of Various Precursors Reacted in 7.3 M Sulfuric Acid

precursors		absorbance maximum (BP/AP) (nm)	maximum PL λ before purification (shoulder) (nm)	maximum PL λ after purification (shoulder) (nm)
o- PDA	glutamic acid	620/532	628 (685)	600 (645, 715)
o- PDA	tryptophan	620/625	628 (684)	637 (693)
o- PDA	none	622/530	630 (686)	598 (642)
o- PDA	PHP	620/530	630 (684)	597 (647)
o- PDA	quinacridone	620/526	628 (684)	548 (588)
p- PDA	glutamic acid	620/380	628 (684)	635 (693)

there is not a large difference in the emission of these products, even when o-PDA is used as the sole precursor, and the degree of aromaticity of the second precursor has no effect. For some reactions, the ratio of blue to red emission was increased (Figure 1C), but this could be due to variation in the purification process. The blue emission was especially dominant for the reaction which used p-PDA, which is unsurprising as this isomer is easily oxidized and does not yield the optimal product. It is clear that o-PDA is an important molecule for this reaction, which may suggest the generation of a larger sp² system built through assembly of o-PDA monomers. Next, the role of the solvent was investigated.

The differences in solvent results provided a more interesting comparison (Table 2). All samples produce similar properties (except 18.2 M sulfuric acid) in terms of red emission, although the relative intensities of the main peaks/ shoulders may have been modified. Even the saturated sodium sulfate solution provides a small amount of the product. To quantify the relative amount of product, the absorption spectrum of each sample was taken after dilution to an appropriate range, and the value for 7.3 M sulfuric acid was taken as 1. These values show that phosphoric acid can produce a similar, though slightly smaller amount of the product, while HCl produces much less than both solvents. This indicates that acid strength does not play a large role in the formation of these CDs. The fact that trace amounts of the product are formed in a saturated sodium sulfate solution indicates that the oxidation capability of the acid's counterion (sulfate, chloride, or phosphate) plays a role in the formation

Table 2. Table Summarizing the Optical Properties and Yields of the Products after Reaction of *o*-PDA and Glutamic Acid in Various Solvents

solvent	absorbance maximum (BP/AP) (nm)	maximum PL λ before purification (shoulder) (nm)	maximum PL λ after purification (shoulder) (nm)	relative yield
7.3 M H ₂ SO ₄	620/532	628 (685)	600 (645, 715)	1.00
7.3 M HCl	621/525	628 (684)	640 (695)	0.06
7.3 M H ₃ PO ₄	620/627	627 (682)	641 (602, 695)	0.60
saturated Na ₂ SO ₄	N/A/534	N/A	600 (647, 715)	N/A
$^{18.2~\mathrm{M}}_{\mathrm{H_2SO_4}}$	431/438	437	473	N/A

of this red-emissive product. Therefore, the presence of an acid and oxidant allows sulfuric and phosphoric acids to be much more efficient in this process than hydrochloric acid.

Proposed Mechanism of Formation. To examine how S-CDs may be forming and the structural moiety responsible for the red emission, we must examine the reaction possibilities for o-PDA in an acidic and oxidative environment. Sulfate and phosphate are not strong oxidants, but there is a great deal of energy applied through raising the temperature to 210 °C. Previous studies have shown one-dimensional oligomers of o-PDA through the use of strong oxidants (persulfate and nitrate) which are on the μ m length scale.^{34,35} Polyaniline is also well known to be prepared through treatment with an oxidant.³⁶ Because of the lower oxidation potential of sulfate/ phosphate, we do not produce larger structures on this scale, but a few units of o-PDA can join together in a branched or linear fashion (Scheme 1). After this oligomerization, the acid present can attack the pyridinic nitrogen and promote crosslinking to convert these nitrogen groups to a graphitic form. The low absolute yield of this reaction indicates that this is not the most favorable reaction and other reactions that involve glutamic acid are more likely to be formed, but these are more water-soluble and so are separated during purification. More branched, polymeric structures of o-PDA are more likely to be water-soluble as well due to the increased number of free amine groups which leads to greater hydrogen bonding in water. It is not believed that glutamic acid plays a significant role in the electronic structure leading to the red emission, but it may play an important role in insulating the sp² islands or providing some polarity to the structure. This compels future studies to more closely compare the product from o-PDA along with the o-PDA/glutamic acid product.

Detection of Water in Organic Solvents. The lack of dispersibility in water as well as the lack of emission from neutral, aqueous solutions suggests the possibility to detect water in organic solvents. Water commonly can contaminate organic solvents, which creates a significant problem if an anhydrous environment is needed for organic reactions. To test S-CDs' ability in this capacity, the same concentration of S-CDs was prepared in ethanol solutions containing different concentrations of water (range: 0-40%), and the PL spectra were recorded with excitation wavelengths of 400 and 500 nm for each sample. The plot of intensity after 500 nm excitation in various water concentrations can be found in Figure 4A and shows a linear trend ($R^2 = 0.95$) indicating the proportional response to water concentration. The error seen in this graph can be attributed to the balance error, and this

Scheme 1. Reaction Scheme Showing the Oligomerization of o-PDA Followed by Conversion to a Crosslinked Network through Formation of Graphitic Nitrogen

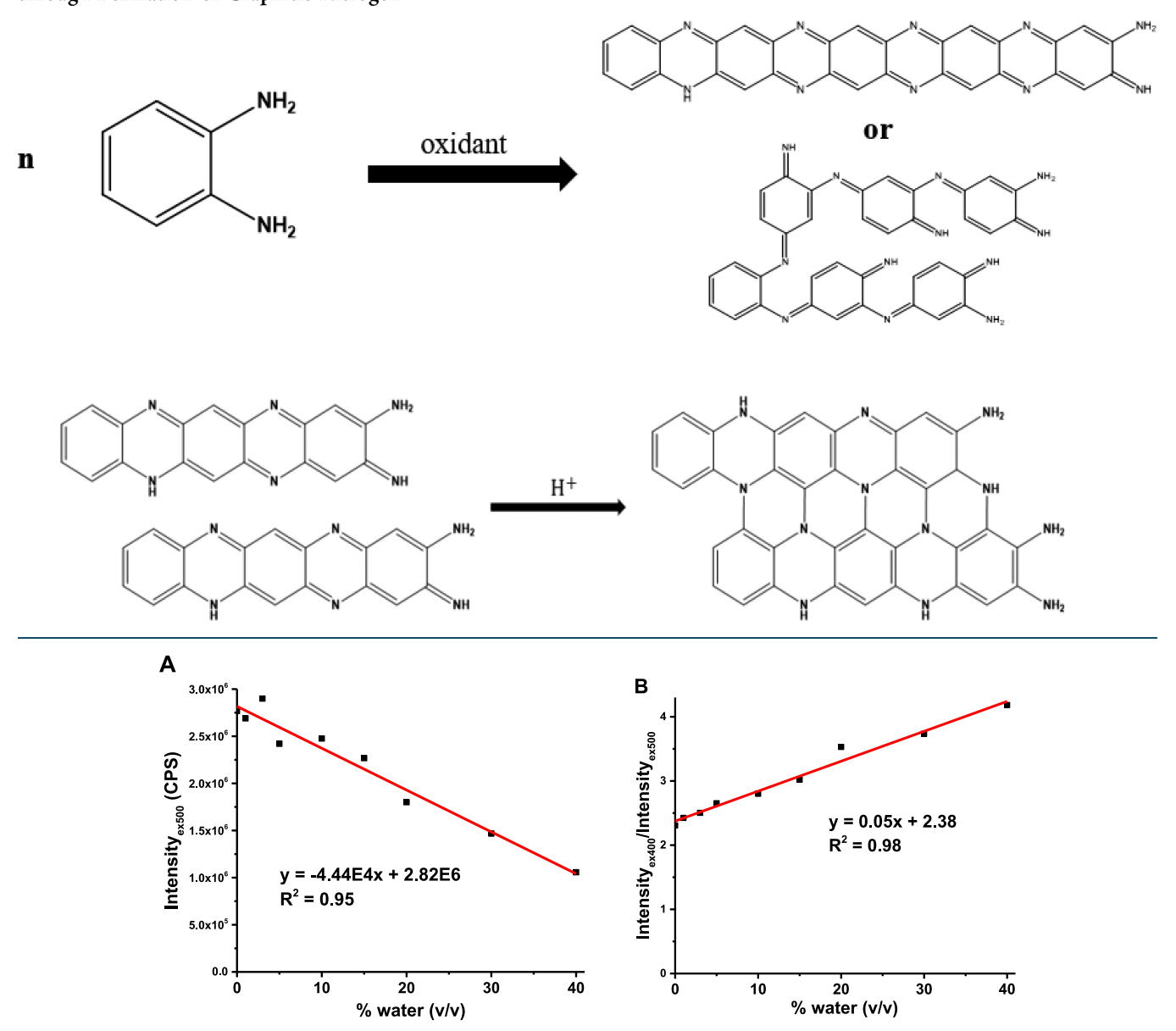
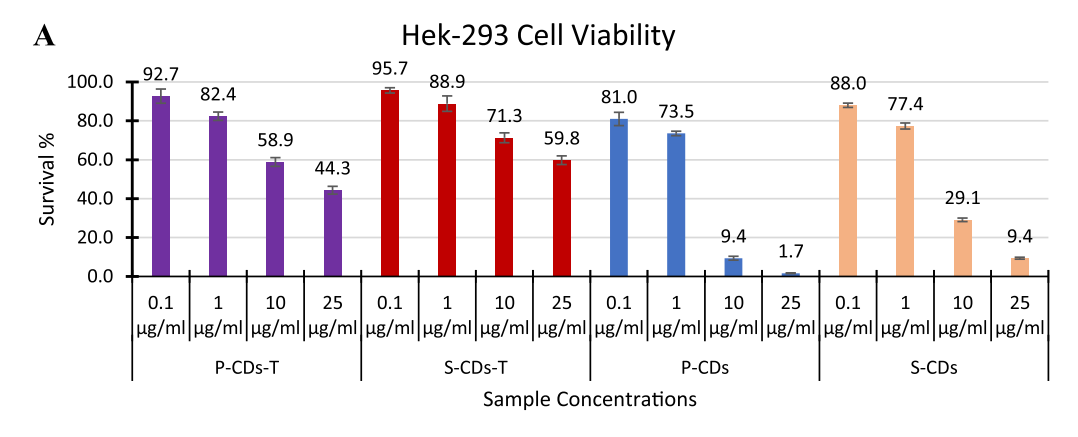


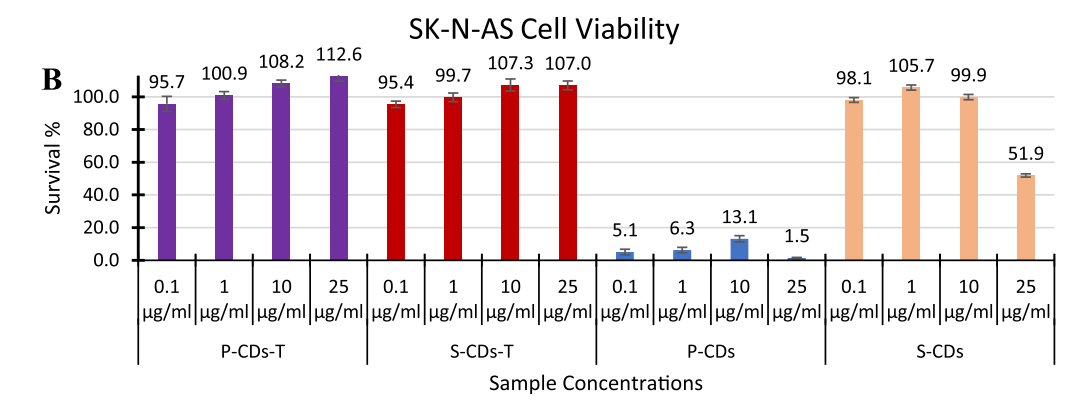
Figure 4. (A) Plot of S-CDs' PL intensity (0.01 mg/mL) versus concentration of water in ethanol upon excitation at 500 nm and (B) ratio of PL intensity upon excitation at 400 and 500 nm in different concentrations of water in ethanol.

can be reduced by dividing two intensities recorded at the different excitation wavelengths (Figure 4B). This graph displays a higher degree of linearity which is because the blue emission is much less sensitive to the presence of water than the orange/red emission and acts similarly to an internal standard to help generate the linear curve which is less sensitive to mass errors. The limit of detection for this method was calculated to be 0.12% or 21.6 mM according to the 3σ method. These results not only provide the ability to detect water, but also suggest that other capabilities may be possible such as pH-dependent emission.

Cytotoxicity Studies of CDs. To evaluate the potential of S-CDs and P-CDs in bioimaging applications, their biocompatibility was evaluated in three cell lines, one nontumor cell line (Hek-293), one N-myc gene-amplified neuroblastoma cell line (SMS-KCNR), and one non-N-myc gene-amplified

neuroblastoma cell line (SK-N-AS). Many other CDs in our lab display a high biocompatibility so it was somewhat surprising to see a higher degree of toxicity for the bare CDs, especially P-CDs. Unique surface groups (S-O/S=O or P-O/P=O) may play some role in this, but it is believed that the hydrophobic nature of these CDs is the largest contributor to the increased toxicity. The lack of hydrophilicity leads to poorly dispersed particles which easily aggregate and could accumulate in or on the cells. Several studies have suggested that a decreased particle size can lead to higher cytotoxicity, but these studies are typically comparing larger sizes than that are relevant for CDs (20 nm to micron size). He lower end of this range (20 nm) is similar to the crystal sizes calculated from the XRD pattern and helps to explain the higher cytotoxicity seen for the CDs in this work.





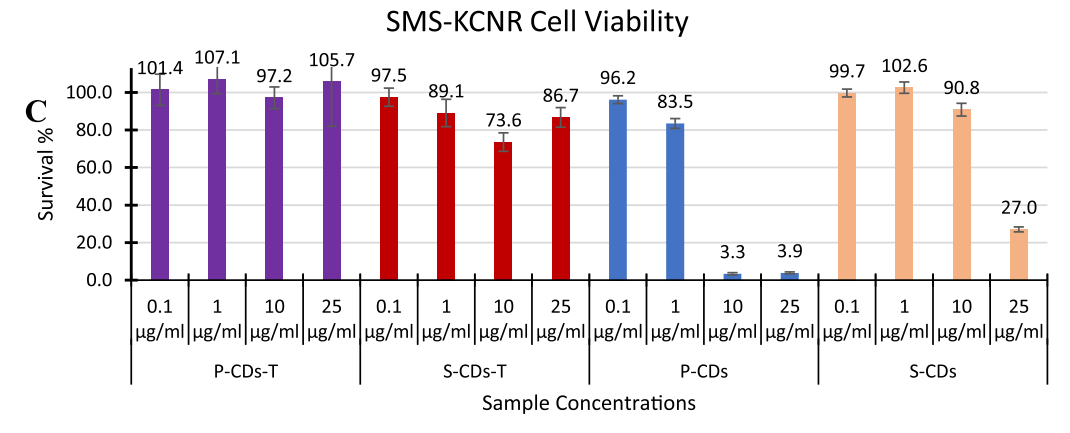


Figure 5. Cytotoxicity studies of CDs. (A) Hek-293 cytotoxicity results. (B) SK-N-AS cytotoxicity results. (C) SMS-KCNR cytotoxicity results. Results are expressed as % of survival rate. Values are means \pm SEM (n = 12). P > 0.05.

Bioimaging is a noninvasive process of visualization of biological activity in a specific period. From that point, when cell apoptosis starts, the cell membrane becomes impaired, and it will tend to take up anything within the media. Thus, any live cell bioimaging materials should be nontoxic toward the targeted cell line. To minimize toxicity from our CDs, a ligand, transferrin was conjugated to the CDs' surface. The data in Figure S2 show successful conjugation, and there are several interesting points to be drawn from these data. First, the absorption spectra were able to be recorded in deionized (DI) water (as opposed to methanol for the bare CDs). This indicates that the ionizable side chains of transferrin are able to increase the dispersity of the conjugate compared to the bare CDs. The absorption peak below 300 nm has shifted closer to 280 nm in the conjugate indicating absorption coming from

tryptophan and other aromatic amino acids, and this peak (and the enhanced tailing at 200 nm) combined with the peak around 600 nm indicates a successful conjugation. The significant shifting and broadening seen for the 600 nm absorption compared to the bare CDs are related to solvent differences, similar to what was discussed previously for the bare CDs in sulfuric acid and methanol. The PL spectra of the conjugates (Figure S2) also show the favorability of the blue emission in water compared to the longer wavelength emission between 600 and 700 nm.

The biocompatibility for these CDs conjugated with transferrin is quite significantly enhanced compared to the bare CDs (Figure 5). S-CDs-T shows an at least 50% more biocompatible response for all the cell lines at the concentrations tested compared to bare CDs, while P-CDs-T

exhibits an at least 40% more biocompatible response compared to S-CDs-T. After conjugation with transferrin, nontumor Hek-293 cells were more sensitive toward the CD treatment compared to SMS-KCNR and SK-N-AS cancer cells. We hypothesized that because of the presence of transferrin receptors, cell uptake rates of CDs should be higher with the cell lines that express transferrin receptors more. Regarding this hypothesis, we performed western blot analysis to show the levels of transferrin receptor 1 (TFR1) on Hek-293, SMS-KCNR, and SK-N-AS cell lines. Figure 6 shows that HEK-293

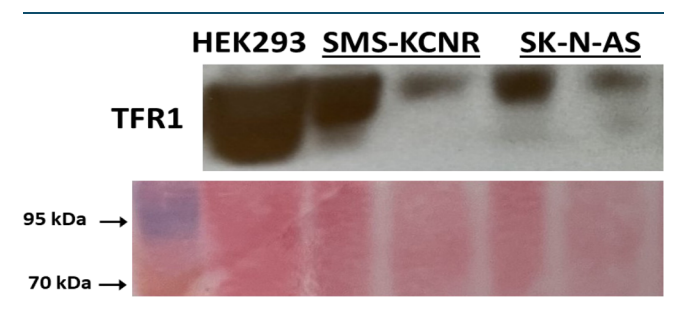


Figure 6. Levels of TFR1 as determined by western blot analysis. Ponceau-stained nitrocellulose blot is shown as a loading control.

expresses the highest level of TFR1 receptors followed by SMS-KCNR and then SK-N-AS. In other words, when we compare the survival rates of cytotoxicity studies, sensitivity levels range from high to low in the order of HEK-293, SMS-KCNR, and SK-N-AS because of the TFR1 expression levels exhibited via western blot assay. The increased water solubility of the transferrin conjugates coupled with the increased biocompatibility indicates the potential of these CDs, particularly S-CDs, in bioimaging studies.

In Vitro Bioimaging Studies with S-CDs and P-CDs. Synthesizing highly efficient red-emissive CDs is still one of the main challenges that draws a significant amount of attention from the scientific community regarding widespread applications of CDs in bioimaging. One of the main reasons that redemissive CDs are highly desirable is that CDs can be excited with longer wavelengths and can penetrate deep in tissue without causing damage to the target cell/tissue/organ, via a truly facile synthesis method. 44 Previous studies have shown that abnormal expression of N-myc genes to the developing nervous system in mouse models has a potent oncogenic effect which results in the development of high-risk neuroblastoma subgroup tumors. 45,46 Additionally, N-myc gene amplification was one of the earliest genetic indicators discovered in neuroblastoma and is still accepted as one of the strongest predictors of poor prognosis. Therefore, to understand fundamentals of neuroblastoma for improved diagnostic and treatment strategies, neuroblastoma subgroup tumors with and without N-myc gene amplification should be studied closely. Thanks to their excellent PL properties and good QY, S-CDs-T and P-CDs-T were employed to image one N-myc geneamplified neuroblastoma cell line SMS-KCNR and one non-Nmyc gene-amplified neuroblastoma cell line SK-N-AS in the red region of light. Here, our control group was treated with only the DAPI nucleus staining agent which can be imaged under the blue channel. Moreover, CDs did not change the cell shape and viability. Figures 7 and 8 show that S-CDs and P-CDs distributed throughout the cell structure, including the nucleus after 1 h of treatment. Because these CDs were conjugated with transferrin, TRF1 plays a significant role regarding the cell

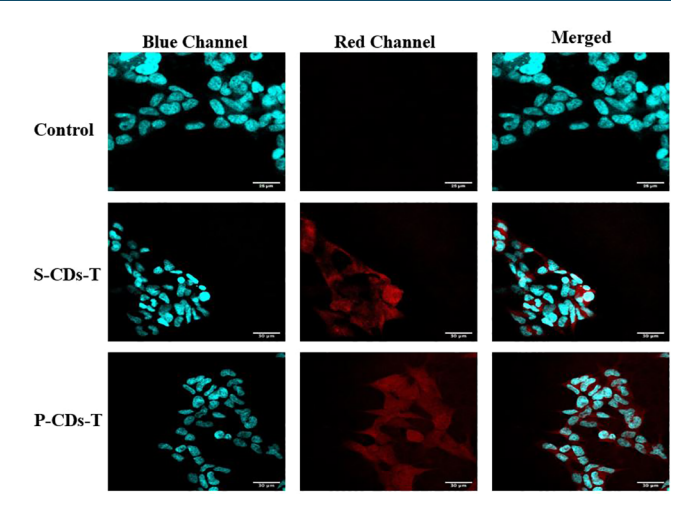


Figure 7. Confocal images of SMS-KCNR tumor cells after incubating with CDs for 1 h. Scale bars are 30 μ m for S-CDs-T and P-CDs-T and 25 μ m for the control. Excitation wavelengths: blue, 405 nm, and red, 561 nm. Emission ranges: blue, 420–460 nm, and red, 615–710 nm.

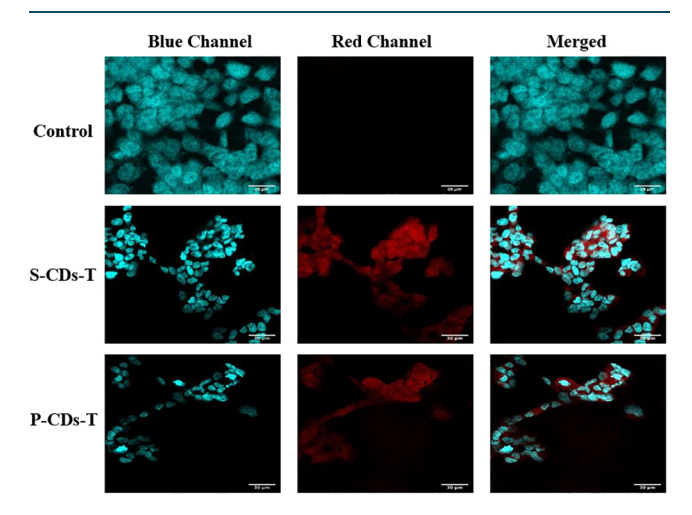


Figure 8. Confocal images of SK-N-AS tumor cells after incubating with CDs for 1 h. Scale bars are 30 μ m for S-CDs-T and P-CDs-T and 25 μ m for the control. Excitation wavelengths: blue, 405 nm, and red, 561 nm. Emission ranges: blue, 420–460 nm, and red, 615–710 nm.

uptake mechanism of the S-CDs-T and P-CDs-T. Conjugation of the CDs with transferrin provided not only a target specific receptor (TFR1)-based cell uptake of these CDs but also increased the water solubility and biocompatibility of CDs for enhanced bioimaging studies. These CDs also display a strong versatility in the wavelength of imaging. Figure S3 displays that green and red channels are both suitable for the imaging of these CDs. Thus, depending on the intended application, these CDs can be employed for bioimaging studies under different excitation wavelengths. The main reason behind this exceptional characteristic is that these CDs possess a broad PL emission range. The sensitivity of these CDs' PL properties to water concentration and pH suggests future applications for diagnostic imaging. As we showed in Figure 6, N-myc geneamplified neuroblastoma cell line SMS-KCNR expresses higher TR1 receptor levels which results in higher selectivity of S-CDs-T and P-CDs-T on this cell line compared to the non-Nmyc gene-amplified neuroblastoma cell line (Figure 5). Similarly, because of the presence of higher TR1 receptors

on N-myc gene-amplified neuroblastoma cell line SMS-KCNR, P-CDs and S-CDs exhibited better cell uptake to all cell structures with higher PL emissions (Figures 7 and 8).

CONCLUSIONS

The need for CDs which show emission in the red region of light is a well-established goal in the current literature. Previous studies have been limited by the QYs in this region as well as dubious reports of water solubility of CDs which display the desired emission in organic solvents. In this work, we built upon previous reports of water-insoluble CDs to understand their formation and increase their water dispersibility and biocompatibility to make them a viable system for biological studies. Through variation of solvents with different acid and oxidative capabilities, we conclude that the important reactions for red emission in this system are the oligomerization of o-PDA and crosslinking of these oligomers to create a large conjugated system containing graphitic nitrogen. The hydrophobicity of these CDs was exploited to quantitatively detect water concentration in ethanol, which may have some use for organic chemists. Finally, the water dispersibility and hence, we believe, the biocompatibility of these CDs were increased through conjugation of transferrin. This led to a nontoxic material which is a versatile imaging agent in fluorescence microscopy. We imaged our transferrin-conjugated CDs on two neuroblastoma cell lines with and without N-myc gene amplification. Thanks to the presence of high TR1 receptors, our CDs showed better PL cell emissions on N-myc geneamplified neuroblastoma cell line SMS-KCNR. Future work may involve the use of this system to deliver therapeutics for the treatment of neuroblastoma and different directions to passivate the surface of S-CDs to increase the hydrophilicity while maintaining maximum brightness of the red emission of light.

■ MATERIALS AND METHODS

Materials. Glutamic acid (99%), o-PDA (99.5%), potassium hydrogen phthalate (PHP), phosphoric acid (85%), and anhydrous ethanol (99.9%) were procured from Sigma-Aldrich (St. Louis, MO). Sulfuric acid (96%) was purchased from ARISTAR (distributed by VWR, Radnor, PA). Hydrochloric acid (38%) was bought from Pharmco (Brookfield, CT). Sodium sulfate (99%) and potassium hydroxide were obtained from VWR (Chester, PA). L-tryptophan (99%) was acquired from MP Biomedicals (Irvine, CA). Dialysis tubing with a molecular weight cutoff (MWCO) of 3500 was bought from Thermo Scientific (Rockford, IL). DI water used was ultrapure (type I) water which was purified using a Millipore Direct-Q 3 water purification system acquired from EMD Millipore Corp. The purified water displayed a surface tension of 72.6 mN m⁻¹, a resistivity of 18.2 M Ω cm, and a pH value of 7.0 \pm 0.3 at 20.0 \pm 0.5 °C. All the chemicals were used as received.

Instrumentation. UV—vis spectra were measured with an Agilent Cary 100 UV—vis spectrophotometer. PL characterization was performed on a Fluorolog HORIBA Jobin Yvon fluorometer with a slit width of 5 nm for excitation and emission. All optical characterization spectra were obtained with quartz cells possessing a pathlength of 1 cm. The attenuated total reflection Fourier-transform infrared spectra were obtained from a FTIR spectrometer (FT-Nicolet 5700, Thermoscientific) equipped with a Smartorbit (Thermoscientific) operating in attenuated total reflectance in a range

between 600 and 4000 cm⁻¹. TGA was performed using a Netzsch TG 209 F3 Tarsus thermomicrobalance while heating under a nitrogen flow from 40 to 1000 °C at a rate of 10 °C/min. XRD patterns were collected with a Phillips X'pert diffractometer that uses a copper source (0.154 nm wavelength). The lattice d-spacing was calculated from the Braggs condition: $2d\sin\theta = n\lambda$, where 2θ is the peak position in the XRD pattern. For the zeta potential measurement of S-CDs, a DLS nano series Malvern Zetasizer (Westborough, MA) was used. To analyze particle size distribution and nanoparticle morphological properties, a JOEL 1200 × TEM and an Agilent 5420 atomic force microscope in the tapping mode were employed.

METHODS

Preparation and Purification of CDs. To begin, 0.11 g of glutamic acid and 0.16 g of o-PDA (1:2 molar ratio) were mixed in 25 mL of 7.3 M sulfuric acid until dissolved. The solution was then transferred to a Teflon-lined stainless-steel autoclave and was heated up to 210 °C for 10 h. At the end of the reaction, the solution was neutralized with a saturated KOH solution and centrifuged at 3000 rpm for 15 min. The supernatant was discarded (based on preliminary characterization), and the salt/precipitate mixture was vacuum-filtered, and the filter paper was washed with DI water during the filtration until the salt was completely removed. The filter was then placed in an oven at 95 °C for 30 min. When the filter paper was dry, it was placed in a dry vacuum filtration system and the paper was rinsed with methanol until the solution passed the filter paper with none of the purple/red color of the CDs. The filtrate was then transferred to a rotary evaporator to remove the methanol and obtain the solid CDs. Further preparations were made with different precursors and solvents, but the molar ratio of the precursors remained the same and the concentration of acid was 7.3 M unless otherwise specified. The purification remained unchanged, except for nonacid solvents which did not require the neutralization step. To maximize yield and simplify the purification process, an alternative strategy was also utilized. After the reaction, the product mixture was directly transferred to a dialysis membrane (MWCO of 3500 Da) and dialyzed against DI water for 3 days. As the solution neutralized, the CDs precipitated, and following the dialysis process, this could be obtained as a powder through lyophilization. This product displayed no differences in the optical properties or functionalization compared to the alternative purification technique.

Conjugation with Transferrin. Eight milligrams of CDs were dissolved in 1 mL of dimethyl sulfoxide. Then 28.45 mg 1-(3-dimethylaminopropyl)-3-ethylcarbodiimide hydrochloride was dissolved in 2 mL of DI water and was mixed into the CD solution. The mixture was stirred at room temperature for 20 min. Then 17.12 mg of N-hydroxysuccinimide dissolved in 1 mL of DI water was added to the mixture. After 20 min of stirring, 5 mg of transferrin dissolved in 2 mL of DI water was added to the solution. The entire mixture was stirred at room temperature overnight. Then the mixture was dialyzed using a 3500 MWCO dialysis bag for 3 days. The DI water was replaced every 4–10 h. The final eluent was collected and frozen at -80 °C and lyophilized for 3 days to obtain the powdered product.

Fluorescence QY Calculations. Fluorescence QY calculations were performed as previously described.²¹ In brief, the

fluorescence quantum yield (φ) was calculated by correlating the integrated area under the fluorescence curve and the absorbance intensity values using Rhodamine-B as the reference standard. UV—vis absorbance measurements of the samples in a 1 cm path length cuvette were performed maintaining the absorbance intensity under 0.05 at 550 nm. Then, fluorescence emission spectra of samples were obtained with a 514 nm excitation wavelength. Average of absorbance intensities and integrated areas for the fluorescence emission spectra were used in the following equation, eq 1:

$$\varphi = \varphi_{R} \times (I/I_{R}) \times (A_{R}/A) \times (n^{2}/n_{R}^{2})$$
(1)

In this equation, φ_{R} , I, A, and n symbols illustrate the literature QY of the standard, the integrated area under the PL curve, absorbance intensity at 550 nm, and the refractive index, respectively. Subscript R is denoted for the reference.

Western Blot Analysis. We employed western blot analysis as described in our previous work. ²² Briefly, Hek-293, SMSR, and SK-N-AS cells were lysed in RIPA buffer and 20 μ g of protein were separated by gel electrophoresis. Proteins were injected into nitrocellulose membranes and immunoblotted with antitransferrin receptor 1 (TFR1, Cell Signaling Technology, Danvers, MA, USA) and anti-α-tubulin (Abcam, Eugene, OR, USA).

Neuroblastoma Cytotoxicity Studies with CDs. For the cytotoxicity studies, one nontumor human embryonic kidney HEK-293 cell line and two neuroblastoma SMSR and SK-N-AS cell lines were employed. HEK-293 (0.5 \times 10⁵), SMSR (1 \times 10^5), and SK-N-AS (1× 10^5) cells were grown in 96-well plates and incubated at 37 °C with 5% CO₂ in 100 µL of Dulbecco's modified Eagle's medium high-glucose medium containing 1% penicillin/streptomycin (Gemini Biosciences, West Sacramento, CA) and supplemented with 10% of fetal bovine serum for 24 h. Then, cells were treated with 100 μ L of different concentrations (0.1, 1, 10, and 25 μ g/mL) of CDs. Cell viability was determined using the CellTiter 96 Aqueous One Solution Cell Proliferation Assay (MTS) (Promega Madison, WI). Cell viability was calculated with MTS assay after 72 h of incubation. Absorbance was measured at 490 nm using a BioTek Synergy HT plate reader.

Neuroblastoma Cell Imaging with CDs. SMSR and SK-N-AS cells were grown at four-well plates (NUNC, Denmark) for imaging at a density of 1×10^5 in 750 μ L Roswell Park Memorial Institute medium (RPMI) and incubated for 24 h for sufficient cell growth. Then, the media were aspirated out, and cells were treated with 500 μ L RPMI solutions containing 25 μ g/mL of CDs and further incubated for 1 h. Once the treatment was completed, cells were washed with PBS and fixed with fresh 4% paraformaldehyde for another 30 min. Subsequently, 4% paraformaldehyde was aspirated out and fixed cells were washed with PBS solution two more times. Then, one drop of antifade reagent with DAPI (Thermo Fisher Scientific, Waltham, MA) was added on the top of the cells. For each well, one cover slip was inserted carefully on top before imaging. A Leica SP5 confocal microscope (Leica Microsystems Inc., Buffalo Grove, IL) was operated for imaging using fluorescent channels with the excitation wavelength of blue, 405 nm, red, 561 nm and emission ranges: blue, 420-460 nm, and red, 615-710 nm. The same experimental settings were used for each group.

Statistical Analysis. Significance of cytotoxicity and cell viability studies were calculated using Student's t-tests for all

pairwise comparisons of the different treatments that were tested. All the results are mentioned as the mean \pm standard error of the mean (SEM). Significance was set at p < 0.05.

ASSOCIATED CONTENT

Supporting Information

The Supporting Information is available free of charge at https://pubs.acs.org/doi/10.1021/acs.bioconjchem.1c00544.

Optical properties of CDs in organic solvents, optical properties of CDs conjugated with transferrin, and confocal images of cells without DAPI staining (PDF)

AUTHOR INFORMATION

Corresponding Author

Roger M. Leblanc — Department of Chemistry, University of Miami, Coral Gables, Florida 33146, United States;
occid.org/0000-0001-8836-8042; Email: rml@miami.edu

Authors

Keenan J. Mintz – Department of Chemistry, University of Miami, Coral Gables, Florida 33146, United States; School of Materials Science and Engineering, Georgia Institute of Technology, Atlanta, Georgia 30332, United States

Emel Kirbas Cilingir – Department of Chemistry, University of Miami, Coral Gables, Florida 33146, United States

Giacomo Nagaro – Department of Chemistry, University of Miami, Coral Gables, Florida 33146, United States; Department of Chemistry, University of Florida, Gainesville, Florida 32611, United States

Suraj Paudyal – Department of Chemistry, University of Miami, Coral Gables, Florida 33146, United States

Yiqun Zhou — Department of Chemistry, University of Miami, Coral Gables, Florida 33146, United States; ⊙ orcid.org/ 0000-0002-6594-9925

Durga Khadka – Department of Physics, University of Miami, Coral Gables, Florida 33146, United States

Sunxiang Huang – Department of Physics, University of Miami, Coral Gables, Florida 33146, United States

Regina M. Graham – Department of Neurological Surgery, Miller School of Medicine, University of Miami, Miami, Florida 33136, United States

Complete contact information is available at: https://pubs.acs.org/10.1021/acs.bioconjchem.1c00544

Author Contributions

*K.J.M. and E.K.C. contributed equally to this work.

Notes

The authors declare no competing financial interest.

ACKNOWLEDGMENTS

R.M.L. acknowledges the support from the National Science Foundation under the grant 1809060 and 2041413. Also, the authors gratefully acknowledge the great support from the University of Miami, USA. R.G. gratefully acknowledges the support of the Florida Department of Health (FDOH), Live Like Bella under grant number 21LO8, the BCURED Foundation, and the Mystic Force Foundation.

REFERENCES

- (1) Duran, N.; Simoes, M. B.; de Moraes, A.; Favaro, W. J.; Seabra, A. B. Nanobiotechnology of carbon dots: A review. *J. Biomed. Nanotechnol.* **2016**, *12*, 1323–1347.
- (2) Wang; Qiu, J. A review of carbon dots in biological applications. *J. Mater. Sci.* **2016**, *51*, 4728–4738.
- (3) Mintz, K. J.; Zhou, Y.; Leblanc, R. M. Recent development of carbon quantum dots regarding their optical properties, photoluminescence mechanism, and core structure. *Nanoscale* **2019**, *11*, 4634–4652.
- (4) Tajik, S.; Dourandish, Z.; Zhang, K.; Beitollahi, H.; Van Le, Q.; Jang, H. W.; Shokouhimehr, M. Carbon and graphene quantum dots: A review on syntheses, characterization, biological and sensing applications for neurotransmitter determination. *RSC Adv.* **2020**, *10*, 15406–15429.
- (5) Shi, X.; Meng, H.; Sun, Y.; Qu, L.; Lin, Y.; Li, Z.; Du, D. Far-red to near-infrared carbon dots: Preparation and applications in biotechnology. *Small* **2019**, *15*, No. 1901507.
- (6) Zhu, Z.; Zhai, Y.; Li, Z.; Zhu, P.; Mao, S.; Zhu, C.; Du, D.; Belfiore, L. A.; Tang, J.; Lin, Y. Red carbon dots: Optical property regulations and applications. *Mater. Today* **2019**, 52–79.
- (7) Lu, S.; Sui, L.; Liu, J.; Zhu, S.; Chen, A.; Jin, M.; Yang, B. Near-infrared photoluminescent polymer—carbon nanodots with two-photon fluorescence. *Adv. Mater.* **2017**, *29*, No. 1603443.
- (8) Yang, X.; Sui, L.; Wang, B.; Zhang, Y.; Tang, Z.; Yang, B.; Lu, S. Red-emitting, self-oxidizing carbon dots for the preparation of white LEDs with super-high color rendering index. *Sci. China: Chem.* **2021**, *64*, 1547–1553.
- (9) Pan, X.; Zhang, Y.; Sun, X.; Pan, W.; Yu, G.; Zhao, Q.; Wang, J. Carbon dots originated from methyl red with molecular state and surface state controlled emissions for sensing and imaging. *J. Lumin.* **2018**, 204, 303–311.
- (10) Mintz, K. J.; Guerrero, B.; Leblanc, R. M. Photoinduced electron transfer in carbon dots with long-wavelength photoluminescence. *J. Phys. Chem. C* **2018**, *122*, 29507–29515.
- (11) Zheng, M.; Li, Y.; Liu, S.; Wang, W.; Xie, Z.; Jing, X. One-pot to synthesize multifunctional carbon dots for near infrared fluorescence imaging and photothermal cancer therapy. *ACS Appl. Mater. Interfaces* **2016**, *8*, 23533–23541.
- (12) Ding, H.; Wei, J. S.; Zhang, P.; Zhou, Z. Y.; Gao, Q. Y.; Xiong, H. M. Solvent-controlled synthesis of highly luminescent carbon dots with a wide color gamut and narrowed emission peak widths. *Small* **2018**, *14*, No. 1800612.
- (13) Wang, Z.; Yuan, F.; Li, X.; Li, Y.; Zhong, H.; Fan, L.; Yang, S. 53% efficient red emissive carbon quantum dots for high color rendering and stable warm white-light-emitting diodes. *Adv. Mater.* 2017, 29, No. 1702910.
- (14) Mintz, K. J. A proposed model explaining the photophysical and microscopic properties of carbon dots; University of Miami, 2021.
- (15) Otte, J.; Dyberg, C.; Pepich, A.; Johnsen, J. I. MYCN function in neuroblastoma development. *Front. Oncol.* **2020**, *10*, 624079–624079.
- (16) Kembhavi, S. A.; Shah, S.; Rangarajan, V.; Qureshi, S.; Popat, P.; Kurkure, P. Imaging in neuroblastoma: An update. *Indian J. Radiol. Imaging* **2015**, *25*, 129–136.
- (17) Maris, J. M. Recent advances in neuroblastoma. N. Engl. J. Med. **2010**, 362, 2202–2211.
- (18) Marshall, G. M.; Carter, D. R.; Cheung, B. B.; Liu, T.; Mateos, M. K.; Meyerowitz, J. G. The prenatal origins of cancer. *Nat. Rev. Cancer* **2014**, *14*, 277–289.
- (19) Cheung, N.-K. V.; Dyer, M. A. Neuroblastoma: Developmental biology, cancer genomics and immunotherapy. *Nat. Rev. Cancer* **2013**, 13, 397–411.
- (20) Maris, J.; Hogarty, M.; Bagatell, R.; Cohn, S. Neuroblastoma. *Lancet* **2007**, *369*, 2106–2120.
- (21) Cilingir, E. K.; Seven, E. S.; Zhou, Y.; Walters, B. M.; Mintz, K. J.; Pandey, R. R.; Wikramanayake, A. H.; Chusuei, C. C.; Vanni, S.; Graham, R. M. Metformin derived carbon dots: highly biocompatible fluorescent nanomaterials as mitochondrial targeting and blood-brain

- barrier penetrating biomarkers. J. Colloid Interface Sci. 2021, 592, 485-497.
- (22) Graham, R. M.; Hernandez, F.; Puerta, N.; De Angulo, G.; Webster, K. A.; Vanni, S. Resveratrol augments ER stress and the cytotoxic effects of glycolytic inhibition in neuroblastoma by downregulating Akt in a mechanism independent of SIRT1. *Exp. Mol. Med.* **2016**, *48*, e210–e210.
- (23) Zhou, Y.; Mintz, K.; Oztan, C.; Hettiarachchi, S.; Peng, Z.; Seven, E.; Liyanage, P.; De La Torre, S.; Celik, E.; Leblanc, R. Embedding carbon dots in superabsorbent polymers for additive manufacturing. *Polymer* **2018**, *10*, 921.
- (24) Gao, D.; Zhao, H.; Chen, X.; Fan, H. Recent advance in redemissive carbon dots and their photoluminescent mechanisms. *Mater. Today Chem.* **2018**, *9*, 103–113.
- (25) Zhu, S.; Song, Y.; Zhao, X.; Shao, J.; Zhang, J.; Yang, B. The photoluminescence mechanism in carbon dots (graphene quantum dots, carbon nanodots, and polymer dots): Current state and future perspective. *Nano Res.* **2015**, *8*, 355–381.
- (26) Wang, J.; Zhu, Y.; Wang, L. Synthesis and applications of redemissive carbon dots. *Chem. Rec.* **2019**, *19*, 2083–2094.
- (27) Mintz, K. J.; Bartoli, M.; Rovere, M.; Zhou, Y.; Hettiarachchi, S. D.; Paudyal, S.; Chen, J.; Domena, J. B.; Liyanage, P. Y.; Sampson, R. A deep investigation into the structure of carbon dots. *Carbon* **2021**, 173, 433–447.
- (28) Wang, D.; Wang, Z.; Zhan, Q.; Pu, Y.; Wang, J.-X.; Foster, N. R.; Dai, L. Facile and scalable preparation of fluorescent carbon dots for multifunctional applications. *Engineering* **2017**, *3*, 402–408.
- (29) Mewada, A.; Pandey, S.; Shinde, S.; Mishra, N.; Oza, G.; Thakur, M.; Sharon, M.; Sharon, M. Green synthesis of biocompatible carbon dots using aqueous extract of Trapa bispinosa peel. *Mater. Sci. Eng., C* **2013**, 33, 2914–2917.
- (30) Viculis, L. M.; Mack, J. J.; Mayer, O. M.; Hahn, H. T.; Kaner, R. B. Intercalation and exfoliation routes to graphite nanoplatelets. *J. Mater. Chem.* **2005**, *15*, 974–978.
- (31) Li, C.; Chen, X.; Shen, L.; Bao, N. Revisiting the oxidation of graphite: Reaction mechanism, chemical stability, and structure self-regulation. *ACS Omega* **2020**, *5*, 3397–3404.
- (32) Zheng, Y.; Zhang, Z.; Li, C. A comparison of graphitic carbon nitrides synthesized from different precursors through pyrolysis. *J. Photochem. Photobiol., A* **2017**, 332, 32–44.
- (33) Holzwarth, U.; Gibson, N. The Scherrer equation versus the 'Debye-Scherrer equation'. *Nat. Nanotechnol.* **2011**, *6*, 534–534.
- (34) Sun, X.; Dong, S.; Wang, E. Formation of o-phenylenediamine oligomers and their self-assembly into one-dimensional structures in aqueous medium. *Macromol. Rapid Commun.* **2005**, *26*, 1504–1508.
- (35) Li, X.-G.; Ma, X.-L.; Sun, J.; Huang, M.-R. Powerful reactive sorption of silver (I) and mercury (II) onto poly (o-phenylenediamine) microparticles. *Langmuir* **2009**, *25*, 1675–1684.
- (36) David, T.; Mathad, J. K.; Padmavathi, T.; Vanaja, A. Part-A: Synthesis of polyaniline and carboxylic acid functionalized SWCNT composites for electromagnetic interference shielding coatings. *Polymer* **2014**, *55*, 5665–5672.
- (37) Chao, D.; Lyu, W.; Liu, Y.; Zhou, L.; Zhang, Q.; Deng, R.; Zhang, H. Solvent-dependent carbon dots and their applications in the detection of water in organic solvents. *J. Mater. Chem. C* **2018**, *6*, 7527–7532.
- (38) Sun, H.; Wang, B.; DiMagno, S. G. A method for detecting water in organic solvents. *Org. Lett.* **2008**, *10*, 4413–4416.
- (39) Thomsen, V.; Schatzlein, D.; Mercuro, D. Limits of detection in spectroscopy. *Spectroscopy* **2003**, *18*, 112–114.
- (40) Park, M. V.; Neigh, A. M.; Vermeulen, J. P.; de la Fonteyne, L. J.; Verharen, H. W.; Briedé, J. J.; van Loveren, H.; de Jong, W. H. The effect of particle size on the cytotoxicity, inflammation, developmental toxicity and genotoxicity of silver nanoparticles. *Biomaterials* **2011**, *32*, 9810–9817.
- (41) Sahu, D.; Kannan, G.; Tailang, M.; Vijayaraghavan, R. In vitro cytotoxicity of nanoparticles: A comparison between particle size and cell type. *J. Nanosci.* **2016**, 1–9.

- (42) Santos, H. A.; Riikonen, J.; Salonen, J.; Mäkilä, E.; Heikkilä, T.; Laaksonen, T.; Peltonen, L.; Lehto, V.-P.; Hirvonen, J. In vitro cytotoxicity of porous silicon microparticles: Effect of the particle concentration, surface chemistry and size. *Acta Biomater.* **2010**, *6*, 2721–2731.
- (43) Emam, A.; Loutfy, S. A.; Mostafa, A. A.; Awad, H.; Mohamed, M. B. Cyto-toxicity, biocompatibility and cellular response of carbon dots—plasmonic based nano-hybrids for bioimaging. *RSC Adv.* **2017**, 7, 23502—23514.
- (44) Karakoçak, B. B.; Liang, J.; Kavadiya, S.; Berezin, M. Y.; Biswas, P.; Ravi, N. Optimizing the synthesis of red-emissive nitrogen-doped carbon dots for use in bioimaging. *ACS Appl. Nano Mater.* **2018**, *1*, 3682–3692.
- (45) Swartling, F. J.; Savov, V.; Persson, A. I.; Chen, J.; Hackett, C. S.; Northcott, P. A. Distinct neural stem cell populations give rise to disparate brain tumors in response to N-MYC. *Cancer Cell* **2012**, *21*, 601–613.
- (46) Swartling, F. J.; Grimmer, M. R.; Hackett, C. S.; Northcott, P. A.; Fan, Q. W.; Goldenberg, D. D. Pleiotropic role for MYCN in medulloblastoma. *Genes Dev.* **2010**, *24*, 1059–1072.

□ Recommended by ACS

Synthesis of Carbon Dots with Carbogenic π -Conjugated Domains for Full-Band UV Shielding

Congcong Chen, Yingliang Liu, et al.

JULY 01, 2022

ACS APPLIED NANO MATERIALS

READ 🗹

Facile Access to Solid-State Carbon Dots with High Luminescence Efficiency and Excellent Formability via Cellulose Derivative Coatings

Kunfeng Jin, Jun Zhang, et al.

MARCH 31, 2020

ACS SUSTAINABLE CHEMISTRY & ENGINEERING

READ 🗹

Carbon Dots Detect Water-to-Ice Phase Transition and Act as Alcohol Sensors *via* Fluorescence Turn-Off/On Mechanism

Sergii Kalytchuk, Radek Zbořil, et al.

MARCH 16, 2021

ACS NANO

READ **C**

Color Emission Carbon Dots with Quench-ResixAstant Solid-State Fluorescence for Light-Emitting Diodes

Fanyong Yan, Jingru Sun, et al.

MARCH 04, 2021

ACS SUSTAINABLE CHEMISTRY & ENGINEERING

READ 🗹

Get More Suggestions >